PANIC

PANIC detector non-linearity correction data

Prepared by	Bernhard Dorner	Max-Planck-Institut für Astronomie
Checked by		

Code: **PANIC-DET-TN-02**

Issue/Ver.: 1.0

Date: **19.02.2015**

No. of pages: 28

Document Change Log

Version	Date	Chapters affected	Comments
Issue 0.1 draft0	16.07.2014	All	Initial draft for preliminary data
Issue 0.1	17.07.2014	All	Minor corrections
Issue 1.0 draft1	02.12.2014	3, 4	Using first CAHA data. Added more plots about data & fitting
		6.2	No test of idlemode and –type recommended any more, added note on data usability.
Issue 1.0	19.02.2015	4	Reduced range to max. 96% saturation. Added plot about true maximum electrons.
		5	Added verification
		6	Using quadrants instead of detectors for indexing extensions
		6.2	Recommended check of DET_ID and DETSEC

List of acronyms and abbreviations

ADU	Analog-digital unit
FPA	Focal Plane Array
GEIRS	Generic Infrared Camera Software
O2K	Omega 2000
PANIC	**PA**noramic **N**ear **I**nfrared camera for **C**alar Alto
QE	Quantum efficiency
SG	Science Grade (detector)

List of supporting documents

The following documents provide additional information about topics addressed in this document. They are referenced as RDx in the text:

RD Nr.	Identifier	Title	Issue	Date
RD 1	PANIC-DET-TR-01	PANIC detector performance	2.0 draft0	01.07.2014
RD 2	PANIC-DET-TN-03	PANIC readout features	1.0 draft0	

RD 3	NTN-2013-004	Description of the NIRSpec linearity correction reference files	1.0	01.11.2013
RD 4	PANIC-SW-TN-04	PANIC FITS headers		
RD 5	PANIC-SW-DCS-01	Generic Infrared Software – Installation and User's Manual		
RD 6	PANIC-DET-TP-01	PANIC list of instrument test procedures	1.0	09.02.2015

Contents

1 INTRODUCTION AND SCOPE

1.1 General

The PANIC Focal Plane Array (FPA) consists of four Teledyne HAWAII-2RG detectors assembled in a 2x2 mosaic. It covers the instrument field of view with a sampling of 4095x4096 pixels.

This document describes the correction of the non-linear response of the detectors.

1.2 Contents

The document is structured into parts covering the effect of non-linear response, the calibration data creation, verification of the calibration, and the reference file format. Parts of it are reproduced in RD 1.

2 NATURE OF THE PROBLEM

HAWAII-2RG near-IR detectors exhibit an inherent non-linear response. It is caused by the change of the applied reverse bias voltage due to the accumulation of generated charge. The effect increases with signal levels, so that the measured signal deviates stronger from the incident photon number at higher levels, and eventually levels out when the pixel well reaches saturation.

The common approach is to extrapolate the true signal $S_t(t)$ from measurements with low values, and fit it as a function of the measured data $S(t)$ with a polynomial of order n:

$$S_t(t) = \sum_{j=1}^{n} c_j \, S(t)^j \tag{1}$$

as long as $S(t)$ is below a maximum limit $S_{\max}$.

3 DATA

The effect was analyzed with flat-field images from the procedure DET_FLAT_3_3 as run on 2014/11/01f. (Table 1). It comprises two sequences of images with rising integration time t from minimal to $t_{max} = 230 \, s$ in a first part, and 240–270 s in a second part.

The average saturation ($S \approx 50,000 \, ADU$) was set to occur at $150s$. The exposure time spans were sampled with a 3 s interval between 3 s and 27 s (9 points), and 10 s in the range 30–270 s (24 points).

Table 1: Procedures for flatfield data

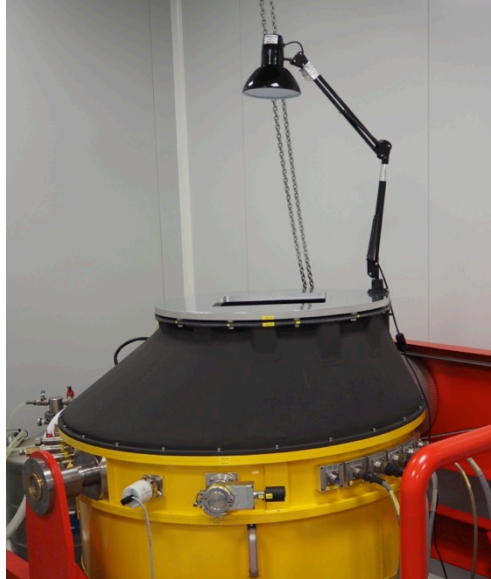| Cycle	Name	Vers.	Date	Content	GEIRS and pattern
7	DET_FLAT	3.3	01/11/2014	Series of flatfields	rjm_r726M-r-s64 (Oct 30 2014, 17:24:44), Panic_r78
	DET_FLAT	3.3	02/11/2014	Series of flatfields, 2nd part	rjm_r726M-r-s64 (Oct 30 2014, 17:24:44), Panic_r78

Figure 1: Lamp lab setup for the flatfield data

The measurements were done at CAHA in the cleanroom in the T3.5m building. A desk lamp with a 15 W light bulb was placed above the instrument entrance (Figure 1), and the Y-bandpass filter in the beam. The lamp was fed with a stabilized power supply and a voltage of 17.8 V. The room was kept dark except for the lamp.

One sequence was read with the lir-mode, the other one with rrr-mpia. The readmodes need individual corrections, since the reset level drifts differently with increasing illumination level (RD 2). These drifts are apparently signal-dependent, and can be compensated with the correction presented here.
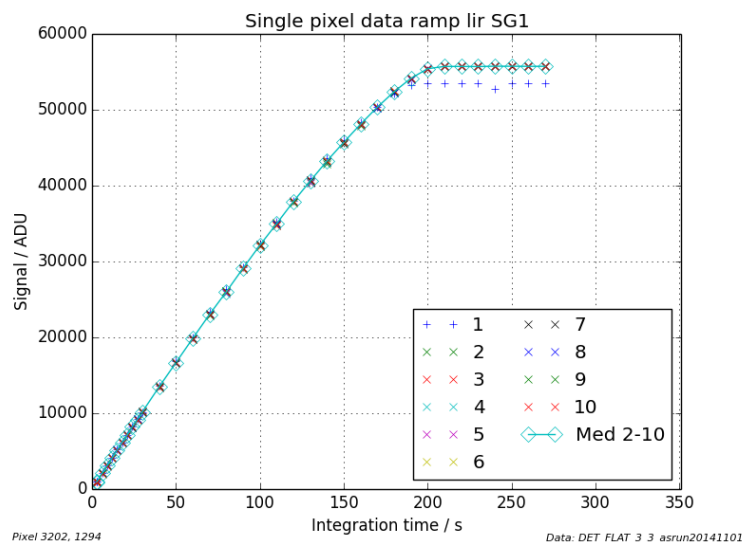

Figure 2: Single pixel ramp of the flatfield data. The first exposure has a wrong reset level and cannot be used.

To increase the SNR per pixel, 10 exposures were recorded for each integration time and numbers 2–10 combined with a median averaging. The first one could not be used because the idle mode was wrongly set to "break", causing the wrong reset level for the first integration, and therefore wrong data (see Figure 2). It is noteworthy that although the second part started with dummy exposures of 230 s to pre-condition the detector, the first 240 s integration deviates more than the 250–270 s ones.

4 ANALYSIS

4.1 Linear extrapolation

4.1.1 Formula and evaluation

In an ideal detector, the signal S_t is a linear function of the exposure time t with offset 0. However, the measured signal S shows a non-linear behavior. This already starts at the very beginning of the integration, but is less pronounced at low signal levels. Nevertheless, a simple linear fit to the data points of the short integration times yields an intercept or $S_t(t = 0)$ far from 0.

A better way to estimate the true linear signal is to fit an exponential function (RD 3) of the form

$$S_e(t) = a + \alpha \left(1 - \exp\left(-\frac{t}{\beta} \right) \right) \tag{2}$$

to data points with small values. When expressing the true signal as

$$S_t(t) = a + bt \tag{3}$$

the parameter a can be taken from the fit of Equation (2), while its derivate at $t = 0$ gives the slope:

$$b = \left. \frac{dS_e}{dt} \right|_{t=0} = \frac{\alpha}{\beta}$$

The exponential fit is created with the data from $t_i = \text{shortest} - 27\,s$ integration time, using points with $S_e < 0.2 \times S(t_{max})$. If less than three points of this group fulfill this criterion, the pixel is skipped and marked as non-correctable (high dark current). The pixel is also marked non-correctable if all the points of the ramp are below 10,000 ADU (low QE).

The approach with the exponential function provided values of b much closer to 0 than standard linear fits for the same data. An example of the exponential fit and the derived linear extrapolation is shown in Figure 3.

Ideally, the intercepts are close to 0, since the data is reset-level corrected. The histograms of the intercepts are shown in Figure 4. Obviously, there is a large spread in the offset at 0 integration time, despite subtracting the reset level. This could result from bias instabilities (RD 2), or pixels with high dark current.
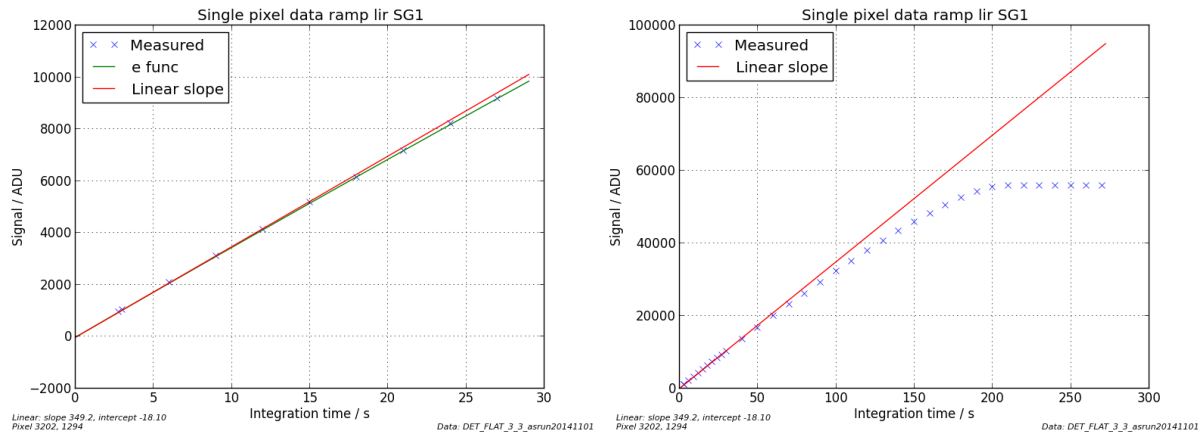
Figure 3: Left: Example of exponential fit to small data points and linear extrapolation showing the nonlinear behavior at low signal levels. Right: Full ramp with linear slope
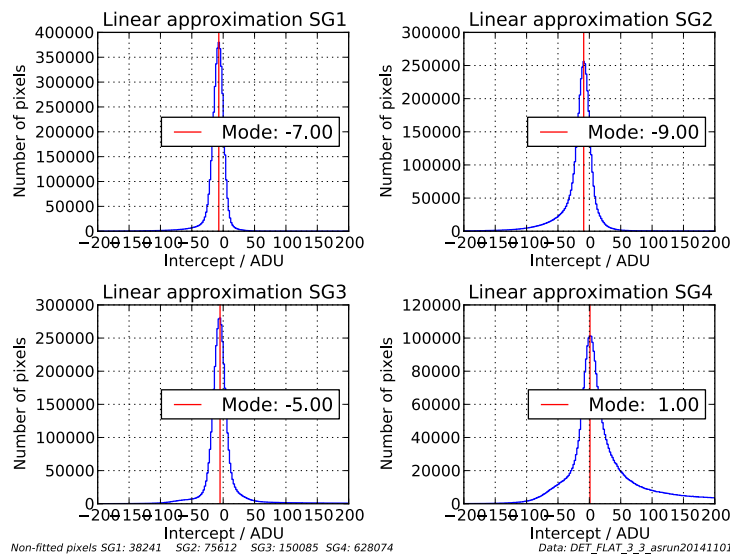
Figure 4: Histogram of linear slope intercepts for 0 integration time

4.1.2 Nonlinear behavior

To illustrate the nonlinear behavior on the full ramp, the relative residual to the linear extrapolation is calculated as $\Delta S_{lin}(t) = (S_t(t) - S(t)) / S_t(t)$. For a single pixel it is shown in Figure 5 left, the median of all pixels in Figure 5 right. Apparently, the ramps are non-linear from the very beginning, crossing the 1% limit at <4,000 ADU, and 5% at <20,000 ADU.

Figure 5: Left: Relative residual to linear extrapolation of a single pixel. Right: Median of all pixels

4.2 Polynomial fit

4.2.1 Principle
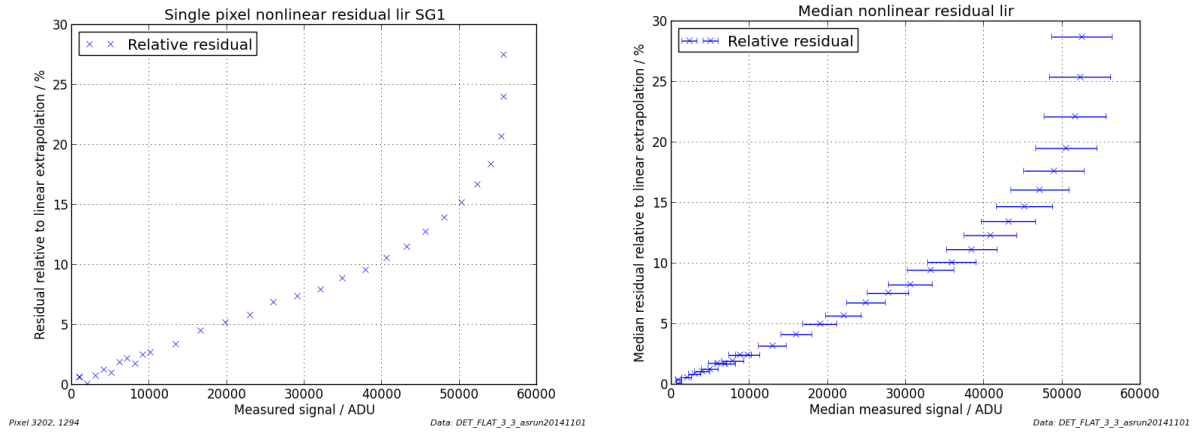
With the linear extrapolation from (3), S_t is calculated for all exposure times t_i. Since the data cannot be corrected once it reaches saturation of the well, and the polynomial cannot perfectly follow the turnoff before, it is necessary to reduce the number of points until a sufficient fit quality is reached.

To achieve a good adaption to the measured data, the fit is done with a 4th order polynomial in the form

$$S_p(t) = c_0 + \sum_{j=1}^{4} c_i\, S(t)^j \tag{4}$$

For each pixel, the polynomial is fitted to the N points with $S(t_i) < 0.98 \times S(t_{max})$[1]. To judge the fit quality, the relative residual is calculated for all integration times as $\Delta S_{rel}(t_i) = \frac{S_p(t_i) - S_t(t_i)}{S_t(t_i)}$.

If the mean value of $\Delta S_{rel}(t_i)$ is < 0.002, and its standard deviation < 0.008 with $i = 3 \dots N$ for lir mode or $i = 2 \dots N$ for rrr-mpia mode, the fit is accepted. If the residual is larger, the last point is excluded and the fit is repeated with the remaining $N_{new} = N_{old} - 1$ points. This is done until a sufficiently small residual is found. If there are only $N = 10$ points left and the residuals are still too large, the pixel is marked non-correctable (unstable or noisy).

If the residual meets the limits, but the correction needed is too large for one of the points, i.e. that $S_t(t_i) > 1.5 \times S(t_i)$ for one $i = 1 \dots N$, the pixel is marked as non-correctable (highly nonlinear behavior or bad linear extrapolation).

The maximum measured value used in the fit $S(t_N)$ is saved, and 98% of this value is set as the maximum correctable signal for this pixel S_{max}.

---

[1] For a new analysis, use only 96% of the saturation. In this version, the 98% were again reduced by 98% in a later adjustment, as written below.

4.2.2 Example data

The data of one example pixel is shown in Figure 6. The left plot displays the linear signal vs. the measured signal. At the end, the pixel runs into saturation. To fit the polynomial, only points below the full well are used.

The right plot shows the relative residuals for the measured data. In lir mode, the points for 2.74 s and 3 s are always further off and not taken into account. Apparently, the correction is not as precise for small values as for large ones. This is not a big problem if the detectors are always operated above 10% of their full well capacity. Points where the saturation is reached have a larger residual and are above the correction limit.
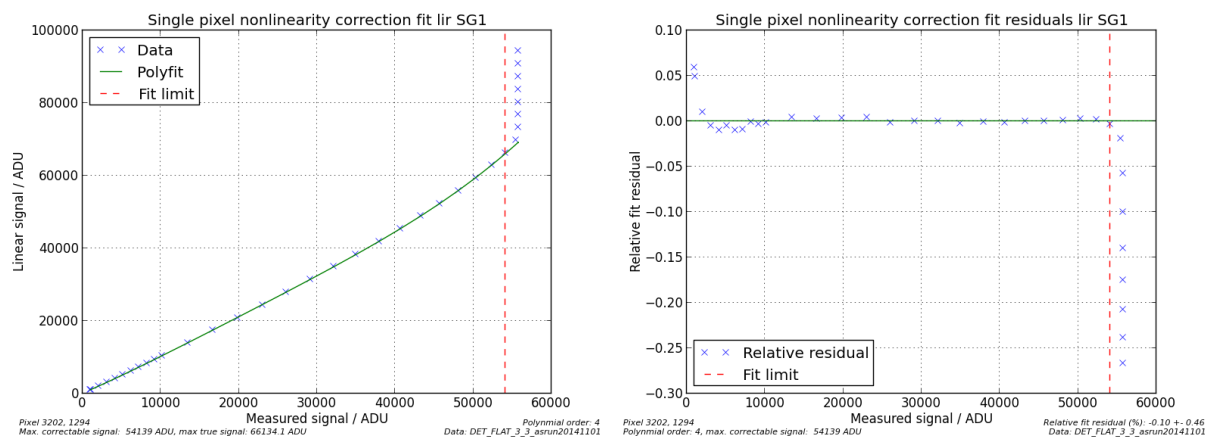

Figure 6: Left: Example of nonlinearity polynomial fit reaching close to saturation. Right: Relative residuals used as cutoff criterion. The points with the two shortest integration times are further off and not taken into account for the cutoff.

4.2.3 Excluded pixels

If the fit with $N = 10$ does not meet the residual criteria, the pixel is marked as non-correctable. If the residuals are small enough, but the correction needed is too large for one of the points, i.e. that $S_t(t_i) > 1.5 \times S(t_i)$ for one $i = 1 \dots N$, the pixel is marked as non-correctable. Pixels with their maximum measured signal $S(t_{\max}) < 10{,}000\ ADU$ are not fitted and marked as non-correctable.

This selection rejects many defects as noisy pixels, high dark current and low QE. In particular the high dark signals caused by the degradation are reliably excluded. Having at least 3 points below 30% fullwell for the linear extrapolation imposes one limit. Rejecting large corrections does a second selection. The degraded pixels show a very nonlinear dark current with a steep initial rise and a approaching a plateau, similar to discharging a capacitor (RD 1). The linear extrapolation there is created from the steep increase at the beginning. The necessary correction then becomes larger and larger for longer integration times. This effect is stronger for higher dark current, so rejecting such pixels is equal to rejecting degraded ones.

The polynomial coefficients $c_{2,3,4}$ for all non-correctable pixels are set to 0, while $c_1 = 1$. To mark them as non-correctable, S_{max} is set to NaN.

4.3 Results

The outputs of the fitting are maps of polynomial coefficients $c_i, i = 1 \ldots 4$ and a map of maximum correctable signal S_{max}. The offset of the polynomials c_0 is not used in the correction.

4.3.1 Readmode lir

The maximum correction limit of all usable pixels in the four detectors is displayed in Figure 7. Most of them are usable up to their full well, a smaller fraction has limits down to 10,000 ADU. Converted to electrons, the limits are in the range of 237–256 ke–.
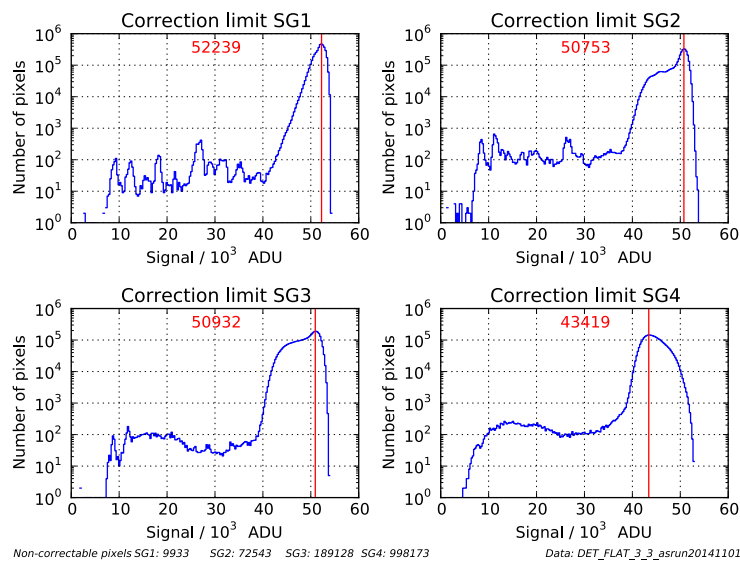

Figure 7: Histogram of maximum correctable signal in readmode lir. The mode values in ADU correspond to 253, 253, 256, 237 ke– for SG1–4.

To better judge the usability of the fit, the histograms are once more created with the correction maximum relative to the full well. As shown in Figure 8, more than 99% of the correctable pixels are usable at least up to 90% of their full well. The remaining ones apparently are not easy to fit with a fourth order polynomial, possibly caused by the nonlinear elevated dark current or noisy outputs.
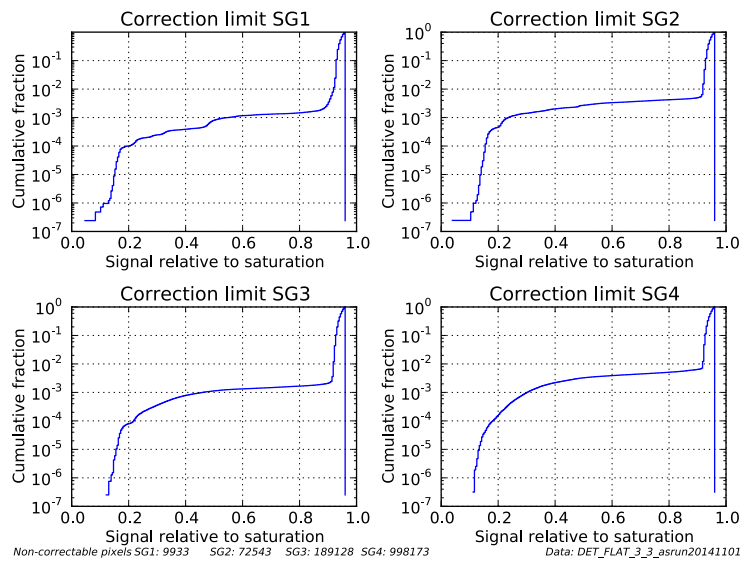
Figure 8: Cumulative histogram of relative maximum correction in lir mode.

The image of the maximum level is plotted in Figure 9. Apart from the clouds of non-correctable pixels in SG4, there are some with low correction limits. They are mostly grouped along the edges of the readout channels and in particular channels, which are possibly noisier. This points to problems with the bias drift, most visible on the start of the fast readout in each channel (RD 2)
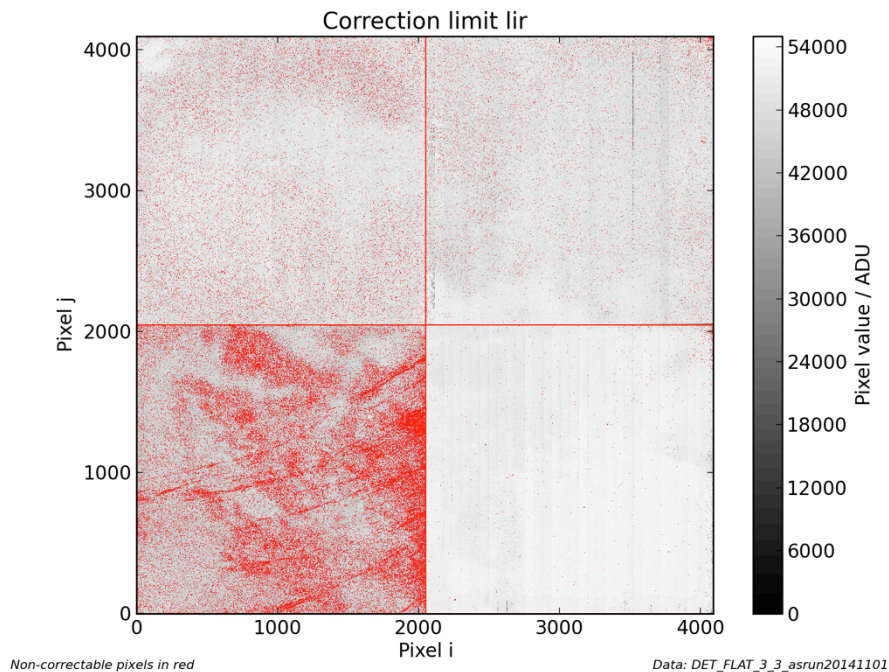
Figure 9: Image of the maximum correction in lir mode, linear scale 0–55,000 ADU. SG1 is bottom right, SG2 top right, SG3 top left, SG4 bottom left. Non-correctable pixels are marked in red. Most apparent are the degraded SG3 and 4 and the reference pixel borders.

To estimate maximum integration times, it is better to use the true maximum correctable signal, i.e. the linearity corrected value of the maximum data from above. These histograms

are plotted in Figure 10. The maxima are around 62,000 ADU, converted to electrons around 290–316 ke– (Table 2).
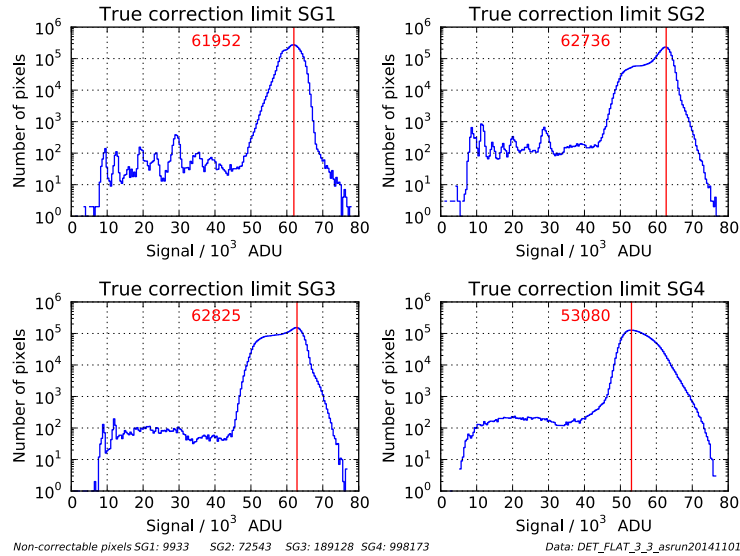

Non-correctable pixels SG1: 9933   SG2: 72543   SG3: 189128   SG4: 998173   *Data: DET_FLAT_3_3_asrun20141101*

Figure 10: Linearity corrected usable limit lir mode. The mode values correspond to 300, 313, 315, and 290 ke–.

Table 2: Usable range in lir mode: CDS counts, and linearized count numbers

Usable range		SG1	SG2	SG3	SG4
Mode	ADU	52,239	50,753	50,932	43,419
	e–	252,837	253,308	255,424	236,590
Mode linearized	ADU	61,952	62,736	62,825	53,080
	e–	299,848	313,115	315,067	289,233

The number of non-correctable pixels per SG is listed in Table 3. The fractions are a little larger than the ones of the hot pixels (RD 1).

Table 3: Amount of uncorrectable active pixels in lir mode (reference pixels excluded).

Quantity	SG1	SG2	SG3	SG4
Number of uncorrectable active pixels	9933	72543	189128	998273
Percentage of active pixels	0.24	1.74	4.54	23.99

The distribution of the polynomial coefficients is shown in Figure 11. The distributions have a well-defined maximum, with slightly larger spread for SG4. The peaks at $c_1 = 1$ and $c_{2,3,4} = 0$ are from the non-correctable pixels.
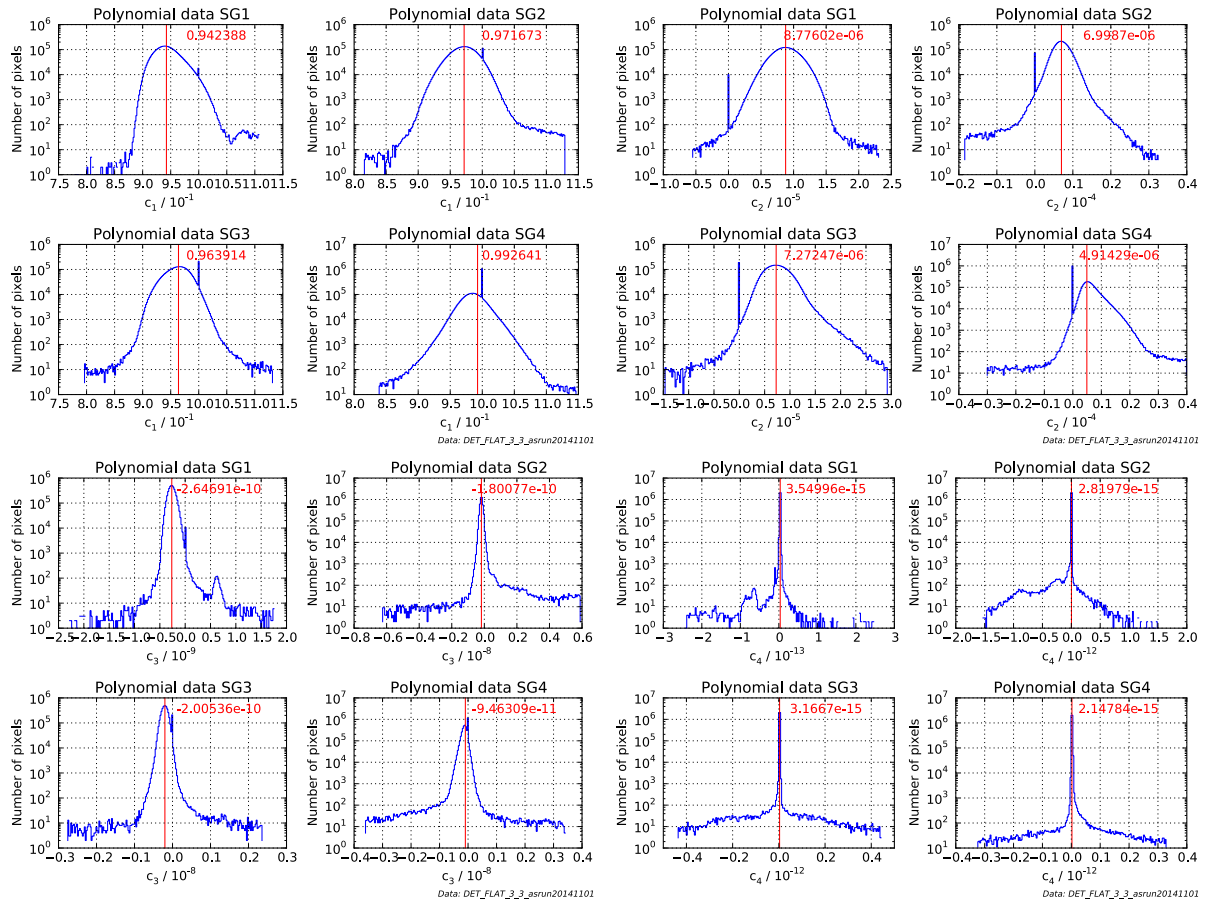
Figure 11: Polynomial coefficients c_1 (to left) to c_4 (bottom right) for readmode lir. The mode is marked with the red line.

4.3.2 Readmode rrr-mpia

The maximum correction limit of all usable pixels in the four detectors is displayed in Figure 12. Most of them are usable close to their full well, a smaller fraction has limits down to 10,000 ADU. Converted to electrons, the limits are in the range of 210–250 ke–. The range is smaller than in lir mode, most likely due to a reduced bias drift at high illumination levels (RD 2).
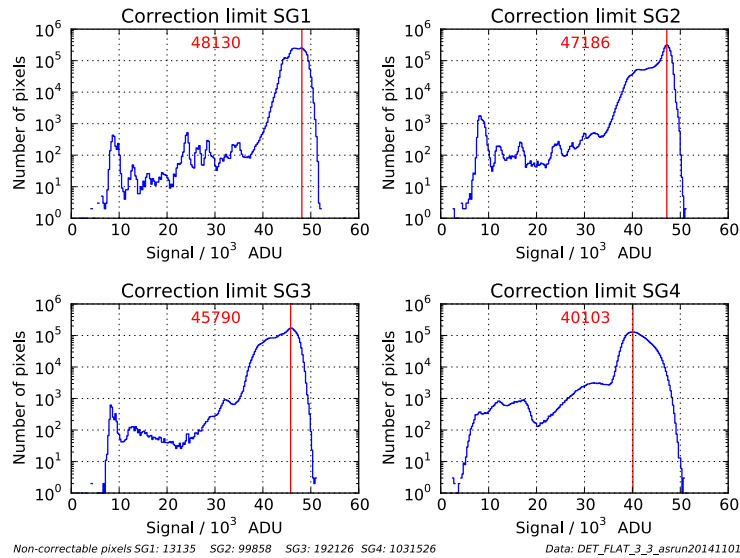
Figure 12: Histogram of maximum correctable signal in readmode rrr-mpia. The mode values in ADU correspond to 233, 227, 223, 216 ke– for SG1–4.

To better judge the usability of the fit, the histograms are once more created with the correction maximum relative to the full well. As shown in Figure 13, more than 99% of the correctable pixels are usable at least up to 90% of their full well in SG1 and 3, and more than 97% up to 90% in SG2 and 4. The remaining ones apparently are not easy to fit with a fourth order polynomial, possibly caused by the nonlinear elevated dark current or noisy outputs.
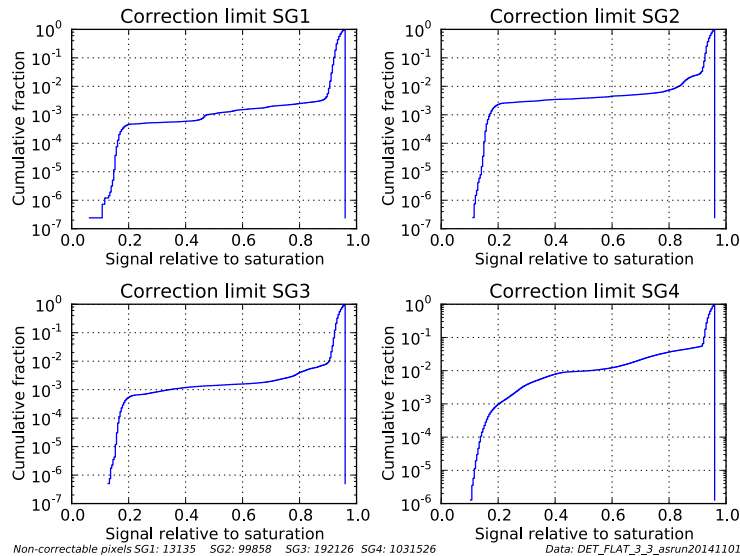

Figure 13: Cumulative histogram of relative maximum correction in rrr-mpia mode.

The image of the maximum level is plotted in Figure 14. Apart from the clouds of non-correctable pixels in SG4, there are some more uncorrectable or with low correction limits. They are mostly grouped along the edges of the readout channels and in particular channels, which are possibly noisier.

Non-correctable pixels in red
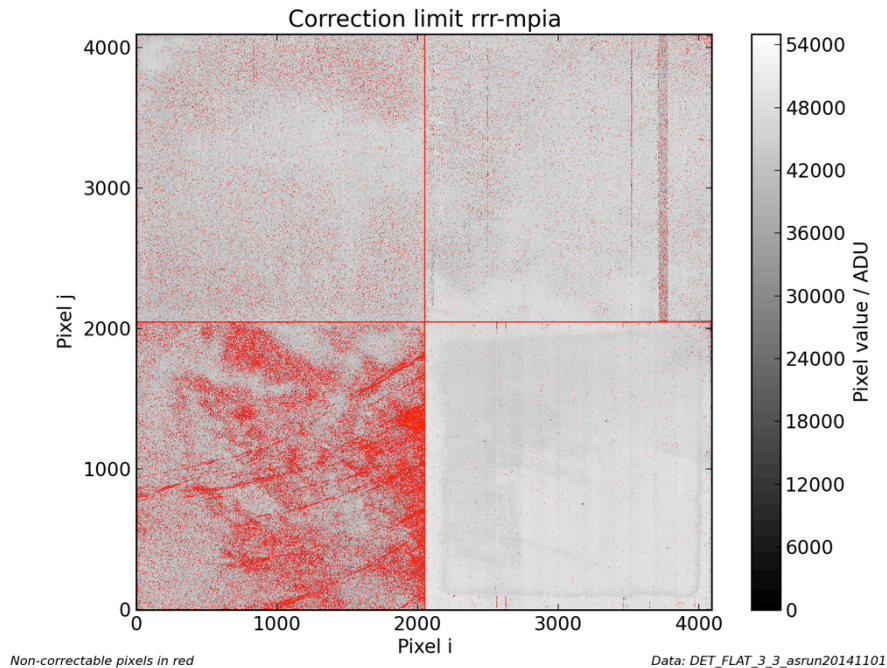
Data: DET_FLAT_3_3_asrun20141101

Figure 14: Image of the maximum correction in rrr-mpia mode, linear scale 0–55,000 ADU. SG1 is bottom right, SG2 top right, SG3 top left, SG4 bottom left. Non-correctable pixels are marked in red. Most apparent are the degraded SG4 and the reference pixel borders, and uncorrectable pixels along readout channels in SG2.

To estimate maximum integration times, it is better to use the true maximum correctable signal, i.e. the linearity corrected value of the maximum data from above. These histograms are plotted in Figure 10. The maxima are around 55,000 ADU, converted to electrons around 265 ke– (Table 4).

Non-correctable pixels SG1: 13135   SG2: 99858   SG3: 192126   SG4: 1031526
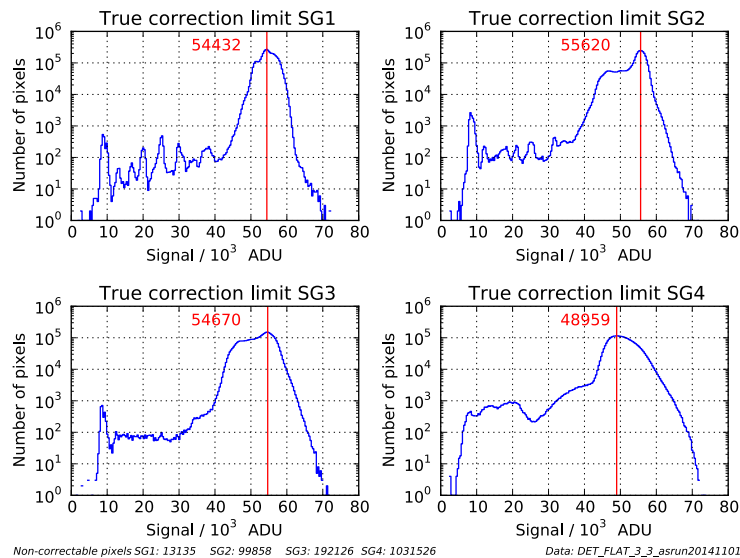
Data: DET_FLAT_3_3_asrun20141101

Figure 15: Linearity corrected usable limit rrr-mpia mode. The mode values correspond to 263, 268, 266, and 263 ke–.

Table 4: Usable range in rrr-mpia mode: CDS counts, and linearized count numbers

Usable range	SG1	SG2	SG3	SG4

Mode	ADU	48,130	47,186	45,790	40,103
	e–	232,949	227,342	222,997	215,703
Mode linearized	ADU	54,432	55,620	54,670	48,959
	e–	263,450	267,977	266.243	263,350

The number of non-correctable pixels per SG is listed in Table 5. The fractions are a little larger than the ones of the hot pixels (RD 1).

Table 5: Amount of uncorrectable active pixels in rrr-mpia mode (reference pixels excluded).

Quantity	SG1	SG2	SG3	SG4
Number of uncorrectable active pixels	13135	99858	192126	1031526
Percentage of active pixels	0.31	2.40	4.62	24.79

The distribution of the polynomial coefficients is shown in Figure 16. The distributions have a well-defined maximum, with slightly larger spread for SG4. The peaks at $c_1 = 1$ and $c_{2,3,4} = 0$ are from the non-correctable pixels.
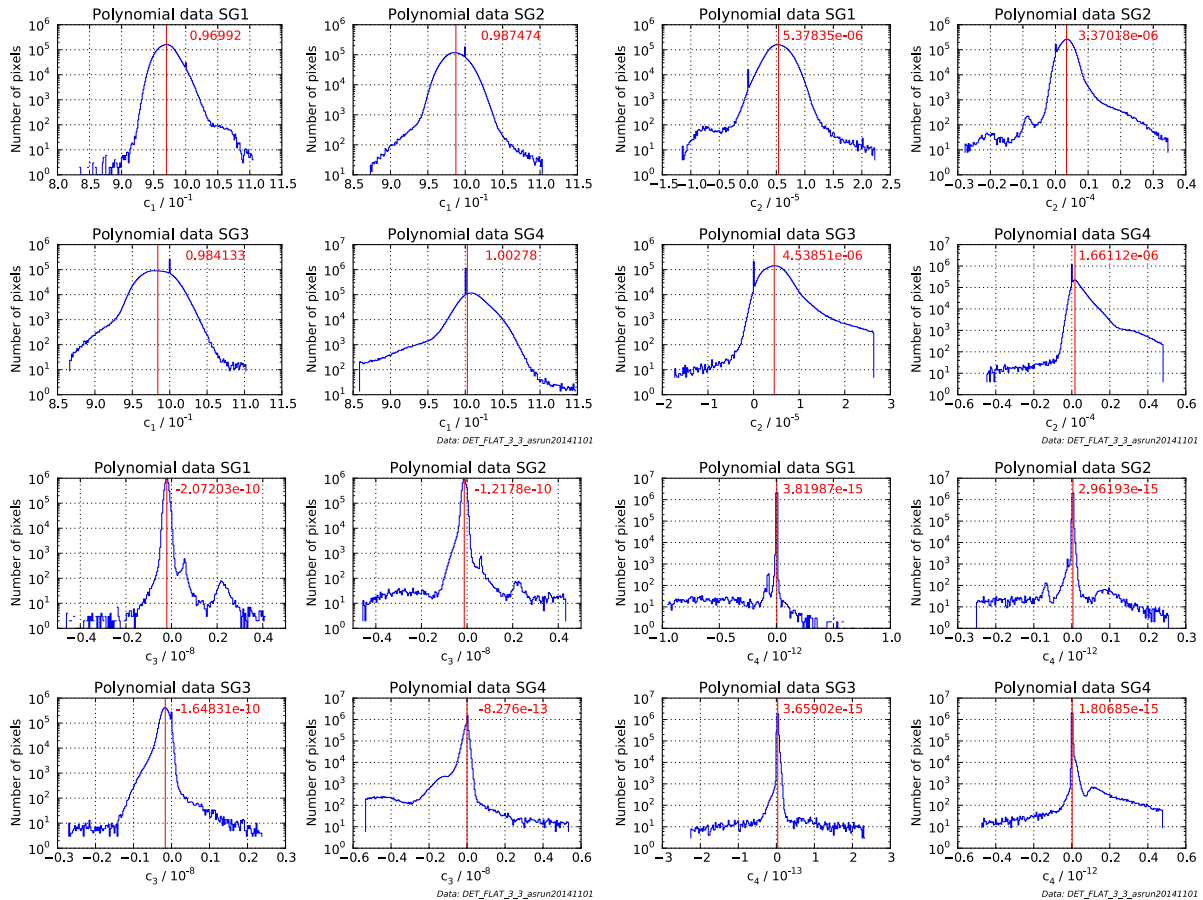

Figure 16: Polynomial coefficients c_1 (to left) to c_4 (bottom right) for readmode rrr-mpia. The mode is marked with the red line.

4.4 Limitations

Although many pixels with high dark current are excluded from the fit, its general nonlinear behavior reduces the accuracy of the correction for all pixels. The dark current is fitted along with the nonlinearity response, but the fit is only done between signals, while the dark current is time dependent. Strictly speaking, this calibration is only applicable for data with the same exposure time and illumination.

However, subtraction of the dark before creating the polynomials would be even worse, as the nonlinear effect is influenced by the accumulated charge. Dark subtracted data would exhibit wrong nonlinear behavior, which is also not valid for other integration times.

Unfortunately it was not possible to use calibration data that saturates in similar times as in operation. The shortest integration times resulted in too high signals, so that the first departure from the linear slope was not reflected in the data. The exponential fit was not working as desired and yielded linear offsets a lot more distant from 0 than with the presented dataset.

Due to the strong influence of the dark current, the calibration has to be repeated if the detector status changes significantly. Therefore, regular monitoring of the pixel status is required. On top of that, the correction should be verified once the instrument starts another cryogenic cycle after having been warmed up. This can be done for example with data from the calibration and a set with short saturation time, as shown below.

Of course, a new calibration always has to be created if the detector operation parameters are modified (timings, voltages).

5 VERIFICATION

5.1 Data

The correction data for this analysis were the files `mNONLIN_LIR_01.01` and `mNONLIN_RRR-MPIA_01.01` created in cycle 7.

To demonstrate the application of the correction for different count rates, images were taken with different light levels with varying exposure times. The datasets are listed in Table 6, for more information see RD 6. The calibration data has been analyzed as well.

Note that newer correction data should not be used for exposures of previous cycles, it is shown below that the results vary depending on the detector status.

The exposures were corrected with the polynomial as in Equation (1). Pixels that are above their maximum correction value were set to NaN, as well if that limit was NaN.

Table 6: Data for verification of nonlinearity correction with various saturation times

Cycle	Name	Vers.	Date	Content	GEIRS and pattern
3	DET_FLAT	3.0	13/06/2014	Series of flatfields, 100 s sat.	rjm_r719M-r-s64 (Jun 11 2014, 12:38:19), Panic_r77M
	DET_LINTEST	1.0	18/06/2014	Series of flatfields, 45 and 200 s sat.	rjm_r719M-r-s64 (Jun 11 2014, 12:38:19), Panic_r77M

6	DET_FLAT	3.2	18/09/2014	Series of flatfields, 30 s sat.	rjm_r724M-r-s64 (Sep 12 2014, 19:54:04), Panic_r78
7	DET_FLAT	3.3	01/11/2014	Series of flatfields, 150 s sat.	rjm_r726M-r-s64 (Oct 30 2014, 17:24:44), Panic_r78
	DET_FLAT	3.3	02/11/2014	Series of flatfields, 2nd part, 150s sat.	rjm_r726M-r-s64 (Oct 30 2014, 17:24:44), Panic_r78
	DET_LINTEST	1.1	07/12/2014	Series of flatfields, 10s sat.	rjm_r729M-r (Dec 5 2014, 09:12:06), Panic_r78M

5.2 Methods

At first, the single images have been corrected, and saved in an up-the-ramp cube. For 10 random pixels in each detector, the original and corrected data is plotted (as long as a correction is allowed for this pixel), along with a linear fit to the corrected points.

To further characterize the correction quality, a linear fit is calculated to the corrected data, while varying the number of included points from the 2 lowest to maximum. In each instance, the relative residual RMS to the line fit is calculated. Besides, the saturation fraction is saved as the fraction of the largest included data point to the last image in the calibration data. A 2D histogram is calculated over the saturation fractions and the residual RMS of all pixels. Each bin in the saturation direction (i.e. each histogram of residuals) is furthermore normalized to its maximum, and the median of the pixel numbers in residual direction is calculated.

5.3 Results

As examples, the results for lir mode are shown. The statements made below are also applicable to rrr-mpia, except where noted differently. The pixel ramps are presented for a random selection in SG2, the residual maps for all available pixels.

5.3.1 Calibration data (150 s saturation)

The plot in Figure 17 left shows the ramps. The measured data are crosses, the corrected ones the dots. The lines are a linear fit to the corrected data. Each ramp is offset from 0 to better distinguish between individual pixels, the nominal 0 is marked with a short line at the y-axis.

The ramps are almost perfectly straight. The varying correction limit is apparent, as well as the different full well capacity and small differences in efficiency or illumination.

The residual map on the right reveals that a substantial fraction of the pixels does not reach a residual <1% after the correction. From 20– 60% saturation, the majority even has residuals of 1–2%. At least the peak in each column lies at values around 0.4%, only at the bright end, the quality decreases.

This is surprising, given that the same data was used to establish the correction. One explanation is that the many points at low signal levels dominate the residuals. As seen in Figure 6 right, the reads <10,000 ADU are a lot more noisier than the others, and deteriorate the fit quality as long as there are few points with higher signal (e.g. in the range to 60%). The cause for the residual increase close to the correction limit is unclear.
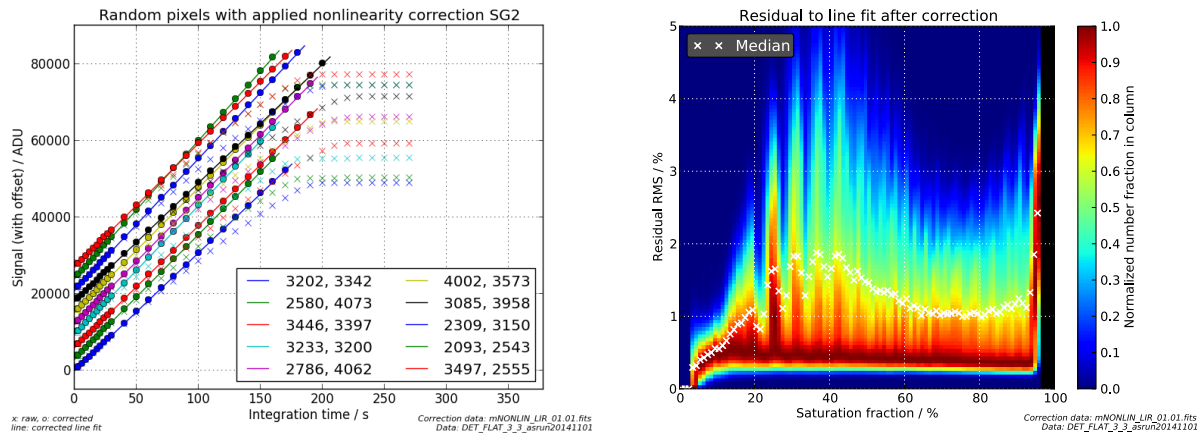

Figure 17: Calibration data (150 s saturation) from cycle 7. Left: 10 pixels ramps SG2, lir. Cross: measured, dots: corrected, line: linear fit. Right: Relative residual depending on saturation fraction, normalized per column.

5.3.2 Bright signals (10 s saturation)

The detectors will rarely be used with long saturation times, in particular for stars. To check the correction with fast integrations, data was taken with the flatfield lamps at the telescope, saturating in about 10 s in the DET_LINTEST 1.1 on 07/12/2014.

The ramps are shown in Figure 18 left. There are fewer points, and the lines are very well matching the data. The residual map on the right proves the high quality of the linear fits, the residuals are typically <1% across the whole range for all pixels. There is some noise at very low fractions <15%, where there are few points in the ramps, mostly from pixels with small response.

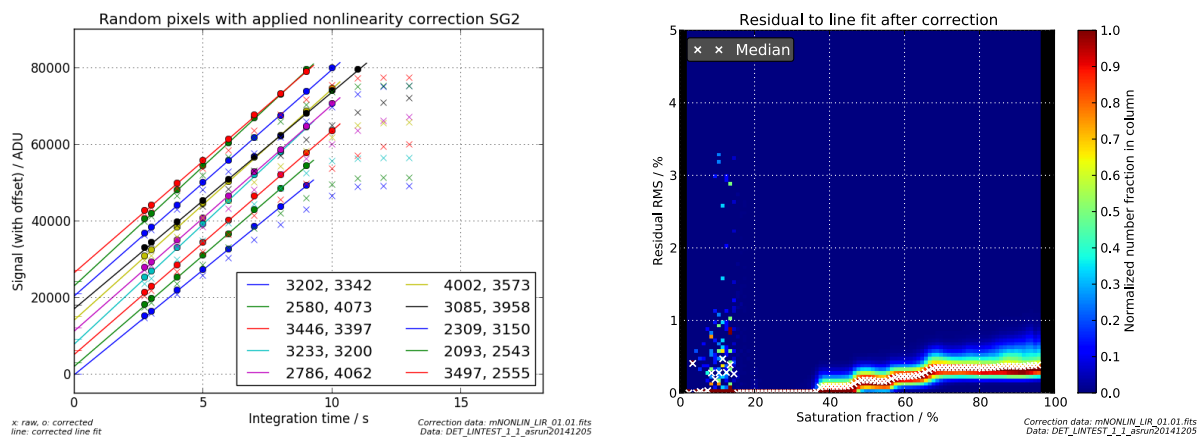**Figure 18: Data with 10 s saturation from cycle 7. Left: 10 pixels ramps SG2, lir. Cross: measured, dots: corrected, line: linear fit. Right: Relative residual depending on saturation fraction, normalized per column.**

5.3.3 Bright signals (30 s saturation)

Another flatfield series with a faster saturation was available from cycle 6, taken in DET_FLAT 3.2 on 18/09/2014. It was planned for deriving linearity information, but the high intensity prevented the necessary small counts in the beginning of the ramps.

The pixel ramps are shown in Figure 19 left. The lines are nicely on the data points, and even cross the y-axis close to their zero point. The residual map shows a good correction of generally <1% RMS, except for very low signals from bad quality pixels.
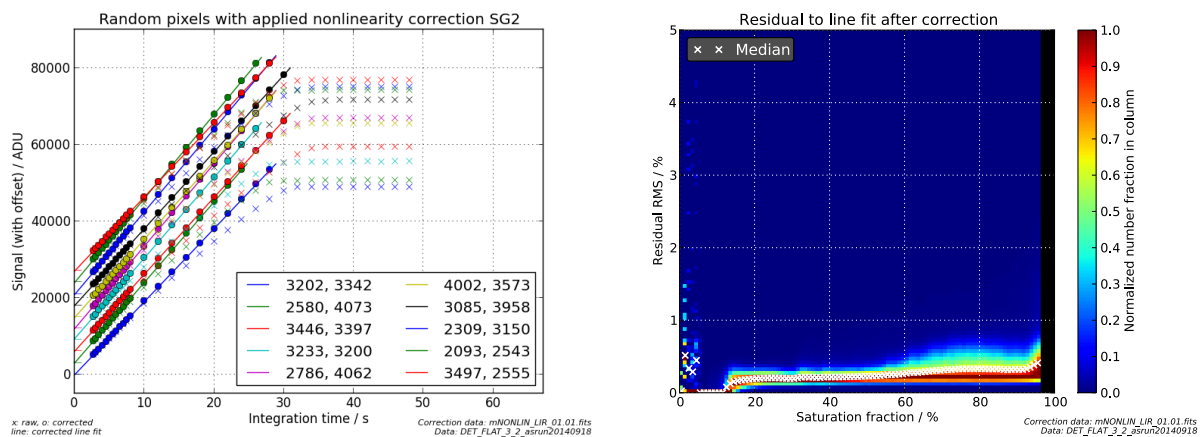

Figure 19: Data with 30 s saturation from cycle 6. Left: 10 pixels ramps SG2, lir. Cross: measured, dots: corrected, line: linear fit. Right: Relative residual depending on saturation fraction, normalized per column.

The rrr-mpia data for this case suffers from unexplained jumps in the ramps, which do not allow a meaningful quality assessment.

5.3.4 Bright signals (45 s saturation)

For testing older data, the DET_LINTEST 1.0 on 18/06/2014 in cycle 3 contains a series reaching saturation within 45 s. However, the focal mask was still installed, and the illumination of the pixels varied strongly in the field.

The ramps in Figure 20 left are straight. The different slopes are due to the uneven intensity on the detector. The residual map on the right confirms a good correction of <1% RMS in the full allowed range, although it is worse than in the newer data.
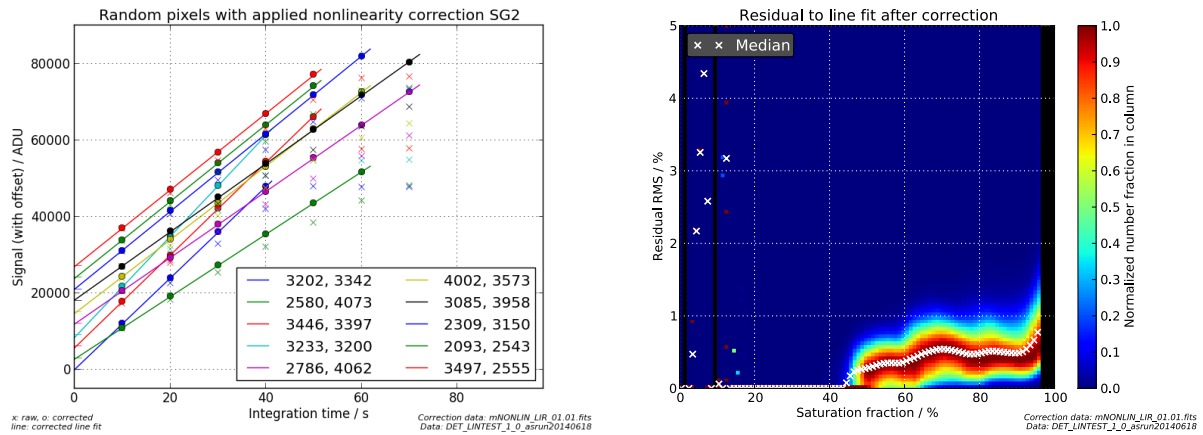
Figure 20: Data with 45 s saturation from cycle 3. Left: 10 pixels ramps SG2, lir. Cross: measured, dots: corrected, line: linear fit. Right: Relative residual depending on saturation fraction, normalized per column.

5.3.5 Brighter signals (100 s saturation)

The first linearity information was derived with the DET_FLAT 3.0 on 13/06/2014, taken in cycle 3. Visually, the ramps on the left in Figure 21 reveal a good match with the linear fits. However, in the residual maps on the right, the quality is significantly worse than for other sets, at the end reaching about 3% RMS. In rrr-mpia, it suddenly even rises to 5% at 80% saturation.

Very low data points, absent in the other examples, may once again affect the quality. Besides, the detector had a different state than in later cycles, most obvious in the hot pixel populations (RD 1). The consequences are apparently less obvious for the 45 s data with fewer points.

Figure 21: Data with 100 s saturation from cycle 3. Left: 10 pixels ramps SG2, lir. Cross: measured, dots: corrected, line: linear fit. Right: Relative residual depending on saturation fraction, normalized per column.

5.3.6 Fainter signals (200 s saturation)

Another test set from older data in the DET_LINTEST 1.0 on 18/06/2014 in cycle 3 saturates in about 200 s. Again, the ramps in Figure 22 left are well met by lines. The residuals are small with <1% RMS, comparable to the 45 s data.
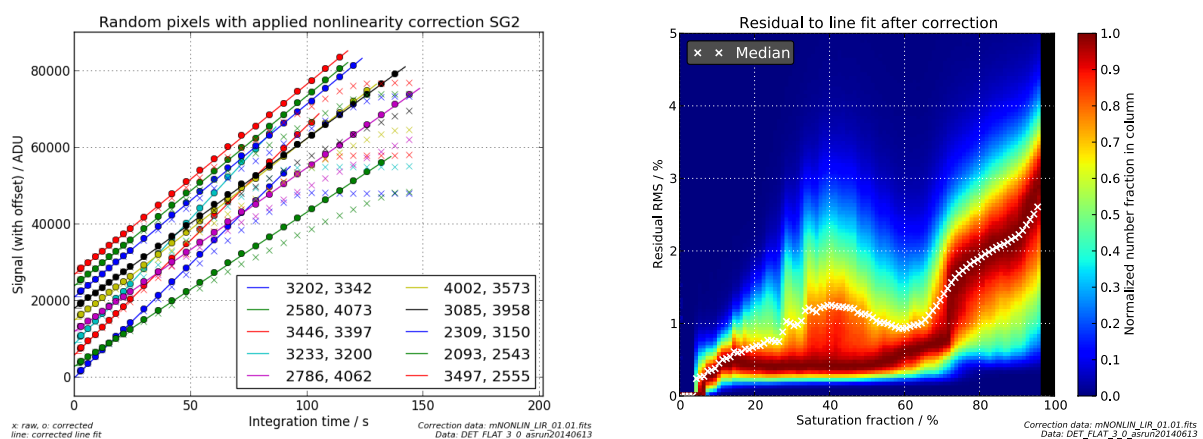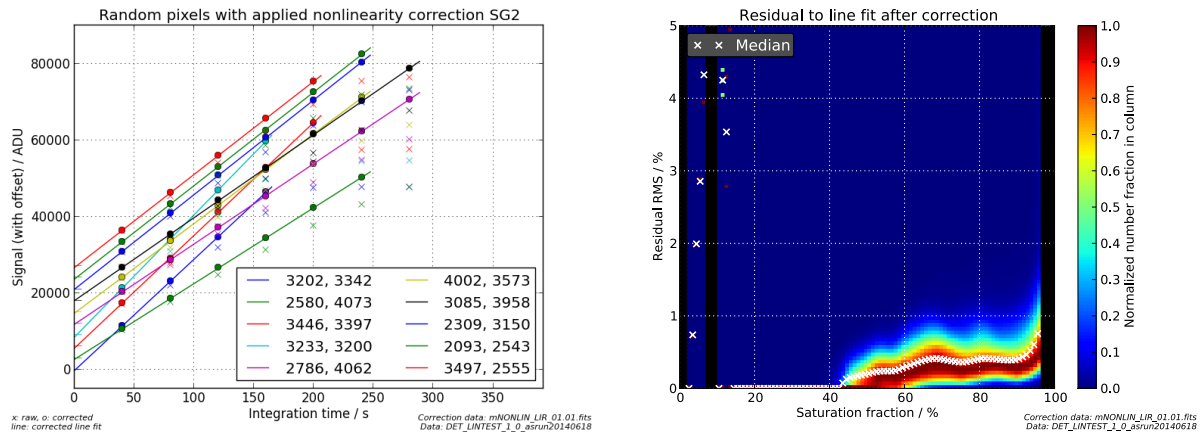
Figure 22: Data with 200 s saturation from cycle 3. Left: 10 pixels ramps SG2, lir. Cross: measured, dots: corrected, line: linear fit. Right: Relative residual depending on saturation fraction, normalized per column.

5.4 Conclusion

The verification demonstrates that the derived correction delivers residuals in the range of 1% RMS, and can be applied to various source intensities, as long as the detector status has not changed. This is emphasized by the example shown in Figure 23, where one pixel has a much higher dark current in old data than in recent one. The residuals also hint at problems at low signal levels, which are apparently noisier. It is not known if that is an effect of naturally low SNR or actual detector instability.
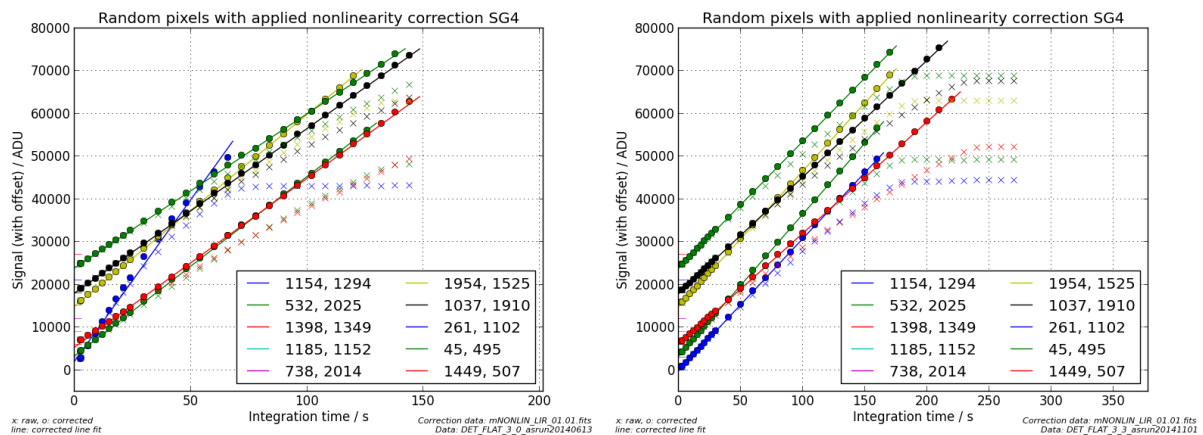
Figure 23: Changed dark current in pixel 1154, 1294. Left: Cycle 3, 100 s saturation. Right: Cycle 7, 150 s saturation. The pixel (blue) is much steeper in the old data, and the new linearity correction is not valid, apparent by the bad match with the line. It is not caused by different relative illumination, since the red pixel 1398, 1349 is close by, and very different from the blue in cycle 3, while being rather similar in cycle 7.

6 REFERENCE FILES

6.1 File format

The fit results are stored in reference files in the FITS data format. The filename is composed as:

`mNONLIN_<readmode>_<version>.fits`

The valid strings are:

- `readmode`: GEIRS read mode in upper case, for now there are "LIR" and "RRR-MPIA"
- `version`: version and subversion as two digit numbers 00-99 separated by a dot, e.g. "01.03".

The FITS file has a primary header with no data, and two data extensions for each detector. They are labeled `LINMAX<i>` and `LINPOLY<i>` with i=1…4 being the quadrant index, numbered similar to the scheme for MEF data files from GEIRS as of this date (RD 4). Note that the indices do not necessarily correspond to SG hardware IDs, which are written in the header instead.

The extension `LINMAX<i>` is a 32bit float 2048x2048 data array containing the maximum correctable signal for each detector. Uncorrectable pixels have a NaN instead of a numerical value.

The extension and `LINPOLY<i>` is a 32bit float 2048x2048x4 data cube containing the polynomial coefficients $c_{1…4}$ in reverse order. The first slice in the cube is c_4, the second c_3, etc.

6.2 Header data

6.2.1 Primary header

The primary header of the file contains data to identify the file type, characterization of the origin data, and parameters of the readout that influence the detector behavior. The entries are listed in Table 7.

Table 7: List of entries in the FITS primary header. The red marked ones can be used to check the applicability of a given file to an exposure.

Key	Value	Comment	Remarks
SIMPLE	T	conforms to FITS standard	Standard
BITPIX	0	number of array dimensions	Standard
NAXIS	0	number of array dimensions	Standard
EXTEND	T		Standard
ID	<filename>		Filename as described in 6.1
AUTHOR	<author name>		Name of creator
DESCR	<Data description>		Short description of file content
INSTRUME	'PANIC'		Instrument name
PAPITYPE	'MASTER_LINEARITY'	File data type as classified by the pipeline	Type of reference data

DATE	<ISO format date string>	UTC date of file creation	Timestamp of file creation
USE_AFT	<ISO format date string>	Use for data taken after this date	Day after which this data has to be used
DETROT90	<number>	[ct] 90 deg SW image rotations	GEIRS rotation value
DETXYFLI	<number>	[1] SW image flip (1=RightLeft, 2=UpDown, 3=bot	GEIRS data flip value
PREAD	<number>	[ns] pixel read selection	GEIRS readout parameter
PSKIP	<number>	[ns] pixel skip selection	GEIRS readout parameter
LSKIP	<number>	[ns] line skip selection	GEIRS readout parameter
READMODE	<read mode string>	read cycle-type	GEIRS readout parameter
IDLEMODE	<idle mode string>	idle to read transition	GEIRS readout parameter, see text
IDLETYPE	<idle type string>	idle cyle-type	GEIRS readout parameter, see text
B_EXT1	<number>	[V] external bias <digital value>	External bias voltage detector 1
B_EXT2	<number>	[V] external bias <digital value>	External bias voltage detector 2
B_EXT3	<number>	[V] external bias <digital value>	External bias voltage detector 3
B_EXT4	<number>	[V] external bias <digital value>	External bias voltage detector 4
B_DSUB1	<number>	[V] det. bias voltage DSUB <digital value>	DSUB voltage detector 1
B_DSUB2	<number>	[V] det. bias voltage DSUB <digital value>	DSUB voltage detector 2
B_DSUB3	<number>	[V] det. bias voltage DSUB <digital value>	DSUB voltage detector 3
B_DSUB4	<number>	[V] det. bias voltage DSUB <digital value>	DSUB voltage detector 4

B_VREST1	<number>	[V] det. bias voltage VRESET <digital value>	Reset voltage detector 1
B_VREST2	<number>	[V] det. bias voltage VRESET <digital value>	Reset voltage detector 2
B_VREST3	<number>	[V] det. bias voltage VRESET <digital value>	Reset voltage detector 3
B_VREST4	<number>	[V] det. bias voltage VRESET <digital value>	Reset voltage detector 4
B_VBIAG1	<number>	[V] det. bias voltage VBIASGATE <digital number>	Bias gate voltage detector 1
B_VBIAG2	<number>	[V] det. bias voltage VBIASGATE <digital number>	Bias gate voltage detector 2
B_VBIAG3	<number>	[V] det. bias voltage VBIASGATE <digital number>	Bias gate voltage detector 3
B_VBIAG4	<number>	[V] det. bias voltage VBIASGATE <digital number>	Bias gate voltage detector 4
HISTORY	Description of creation		Comments on data origin and info
HISTORY	DOCUMENT:		
HISTORY	<Reference TN ID + version>		ID if the reference document + version number
HISTORY	SOFTWARE:		
HISTORY	<script name and version>		Filename of creation script and version
HISTORY	DATA:		
HISTORY	First FILE_ID: <ID>		FILE_ID string of first exposure used for data creation
HISTORY	Last FILE_ID: <ID>		FILE_ID string of last exposure used for data creation
HISTORY	<GEIRS info string>		CREATOR entry in the

			exposure header
HISTORY	DIFFERENCES:		
HISTORY	<Version info>		Comment on differences to previous version

The data marked in light red should be checked and compared with the data of the exposure to correct, i.e. if the correction data is applicable to this file (instrument, USE_AFT) and if the data orientation and readout parameters are the same. The version of the readout pattern is only noted in the HISTORY <GEIRS info string>, as it may change without changing the timings and voltages.

The values of IDLEMODE and IDLETYPE do not have to be checked. However, the correction is only valid for data that are read after reading at least one full image to assure the correct reset level. This can be achieved by using idlemode "wait" and idletype "ReadWoConv", as described in RD 5. If any other mode or type is set, all data but the first read can be used and corrected the same way.

6.2.2 LINMAX<i> extension

The header of the LINMAX<i> extensions has some keywords to identify the detector and the section in a full-frame image. They are listed in Table 8.

Table 8: List of entries in the LINMAX<i> extension header. The red marked ones can be used to check the applicability of a given file to data.

Key	Value	Comment	Remarks
XTENSION	'IMAGE'	Image extension	Standard
BITPIX	-32	array data type	Standard
NAXIS	2	number of array dimensions	Standard
NAXIS1	2048		Standard
NAXIS2	2048		Standard
PCOUNT	0	number of parameters	Standard
GCOUNT	1	number of groups	Standard
EXTNAME	'LINMAX<i>'	extension name	Ext. name with quadrant index i
BUNIT	'ADU'		Unit of data
DESCR	'Max level for linearity correction'		Description of data
DETSEC	'[imin:imax,jmin:jmax]'		Data section in full frame image
DET_ID	'SG<i>'		Detector hardware ID

6.2.3 `LINPOLY<i>` extension

The header of the `LINPOLY<i>` extensions has some keywords to identify the detector and the section in a full-frame image. They are listed in Table 9.

Table 9: List of entries in the `LINPOLY<i>` extension header. The red marked ones can be used to check the applicability of a given file to data.

Key	Value	Comment	Remarks
XTENSION	'IMAGE'	Image extension	Standard
BITPIX	-32	array data type	Standard
NAXIS	3	number of array dimensions	Standard
NAXIS1	2048		Standard
NAXIS2	2048		Standard
NAXIS3	4		Standard
PCOUNT	0	number of parameters	Standard
GCOUNT	1	number of groups	Standard
EXTNAME	'LINPOLY<i>'	extension name	Ext. name with quadrant index i
DESCR	'Polynomial coefficients (highest first), no offset'		Description of data
DETSEC	'[imin:imax,jmin:jmax]'		Data section in full frame image
DET_ID	'SG<i>'		Detector hardware ID